Available online at www.sciencedirect.com
SCIENCE DIRECT®
Journal of Solid State Chemistry 177 (2004) 3909–3917
JOURNAL OF SOLID STATE CHEMISTRY
www.elsevier.com/locate/jssc

$Pb(UO_2)(V_2O_7)$, a novel lead uranyl divanadate

S. Obbade*, C. Dion, M. Saadi, S. Yagoubi, F. Abraham

Laboratoire de Cristallochimie et Physicochimie du Solide, Universite de Sciences et Technologies de Solide, UMR CNRS 8012, ENSCL-USTL, BP 108, 59652 Villeneuve d'Ascq Cedex, France

Received 14 April 2004; received in revised form 23 June 2004; accepted 9 July 2004
Available online 18 October 2004

Abstract

A new lead uranyl divanadate, $PbUO_2(V_2O_7)$, has been synthesized by high temperature solid-state reaction and its crystal structure was solved by direct methods using single-crystal X-ray diffraction data. It crystallizes in the monoclinic system with space group $P2_1/n$ and following cell parameters: $a=6.9212(9)$ Å, $b=9.6523(13)$ Å, $c=11.7881(16)$ Å, $\beta=91.74(1)^\circ$, $V=787.01(2)$ Å^3, $Z=4$, $\rho_{mes}=5.82(3)$, $\rho_{cal}=5.83(1)$ g/cm^3. A full-matrix least-squares refinement on the basis of F^2 yielded $R_1=0.029$ and $wR_2=0.064$ for 2136 independent reflections with $I>2\sigma(I)$ collected with a Bruker AXS diffractometer (Mo$K\alpha$ radiation). The crystal structure of $PbUO_2(V_2O_7)$ consists of a tri-dimensional framework resulting from the association of V_2O_7 divanadate units formed by two VO_4 tetrahedra sharing corner and UO_7 uranyl pentagonal bipyramids and creating one-dimensional elliptic channels occupied by the Pb^{2+} ions. In $PbUO_2(V_2O_7)$, infinite ribbons of four pentagons wide are formed which can be deduced from the sheets with Uranophane type anion-topology that occurs, for example, in the uranyl divanadate $(UO_2)_2(V_2O_7)$, by replacement of half-U atoms of the edge-shared UO_7 pentagonal bipyramids by Pb atoms. Infrared spectroscopy was investigated at room temperature in the frequency range 400–4000 cm^{-1}, showing some characteristic bands of uranyl ion and of VO_4 tetrahedra.

Keywords: Lead uranyl vanadate; Crystal structure refinement; Solid-state synthesis; Lone-pair localization

1. Introduction

The lead uranyl vanadates are particularly well-known through the Francevillite $(Pb–Ba)(UO_2)(V_2O_8)\cdot xH_2O$ [1–6] which is an important secondary uranium ore with a constant Pb/Ba proportion. The pure Ba and Pb species have been synthesized, they form a solid solution in all proportions and the Pb variety was named Curienite [4]. These compounds are related with the Carnotite family $K_2(UO_2)_2V_2O_8\cdot H_2O$ where K^+ ion can be replaced by other monovalent ions such Na^+, Rb^+, Cs^+, NH_4^+, Tl^+, Ag^+ [7–15]. There are numerous known divalent compounds $M(UO_2)_2V_2O_8$ with $M=$ Mn, Fe, Co, Ni, Cu, Zn, Cd [16–18]. All these compounds present a layered structure with identical $[UO_2(VO_4)]^-$ infinite sheets, which can be more precisely written $^2_\infty[(UO_2)_2V_2O_8]^{2-}$, where $V_2O_8^{6-}$ centrosymmetric units, formed by two edge-shared VO_5 square pyramids, are associated with UO_2^{2+} uranyl ions, in pentagonal bipyramidal environment. The vanadium square pyramidal coordinan has been also observed in the $CsUO_2(VO_3)_3$ compound [19] which is characterized by $^2_\infty[UV_3O_{11}]^-$ infinite sheets built from VO_5 square pyramids and UO_8 hexagonal bipyramids sharing edges and corners. Similar layers are also observed in UV_3O_{10} [20].

In the majority of recently synthesized uranyl vanadates, the vanadium atoms are observed in tetrahedral coordination [21–27]. Thus, the crystal structure of the pentahydrated uranyl orthovanadate, $(UO_2)_3(VO_4)_2\cdot 5H_2O$ [21] is characterized by $^2_\infty[(UO_2)(VO_4)]^-$ parallel layers, formed by $^1_\infty[UO_5]$ infinite uranium chains connected together by sharing equatorial edges and corners with VO_4 tetrahedra, and these layers are linked by another uranyl ion and by water molecules to

*Corresponding author. Fax: +33-3-20-43-68-14.
E-mail address: obbade@ensc-lille.fr (S. Obbade).

0022-4596/$ - see front matter © 2004 Elsevier Inc. All rights reserved.
doi:10.1016/j.jssc.2004.07.055

form a three-dimensional framework. In the $M_6(UO_2)_5(VO_4)_2O_5$ (M = Na, K, Rb) family [22,23], the crystal structure of sodium and potassium compounds [22] is characterized by uranyl vanadate layers, formed by $^1_\infty[(UO_5)O_{11}]$ infinite ribbons, connected together by VO_4 tetrahedra. In both structures, all vanadium tetrahedra on one side or on the other side of each uranyl ribbon are, respectively, pointed up or pointed down, to give a piling of parallel and corrugated layers $^2_\infty[(UO_2)_5(VO_4)_2O_5]^{6-}$. With rubidium metal, two allotropic α and β forms of $Rb_6(UO_2)_5(VO_4)_2O_5$ forms have been obtained (23), where the β variety crystallizes with corrugated layers identical to those of K and Na compounds, while for the α compound, the VO_4 tetrahedra are alternately inverted along each $^1_\infty[(UO_5)O_{11}]$ row, giving $^2_\infty[(UO_2)_5(VO_4)_2O_5]^{6-}$ planar layers. Two other uranyl vanadates families with V^{5+} in tetrahedral coordination were recently evidenced, the oxychloro uranyl vanadates $M_7(UO_2)_8(VO_4)_2O_8Cl$ with M = Rb, Cs (24) and $M(UO_2)_4(VO_4)_3$ (M = Na, Li) compounds [25]. In the first family, the crystal structure is characterized by $^2_\infty[(UO_2)_8(VO_4)_2O_8Cl]^{7-}$ layers built up from VO_4 tetrahedra, UO_7 and UO_6Cl pentagonal bipyramids, and UO_6 distorted octahedra. While the second family is characterized by $^2_\infty[(UO_2)_2(VO_4)_3]$ sheets parallel to (001) formed by corner-shared UO_6 distorted octahedra and $V(2)O_4$ tetrahedra, connected by $V(1)O_4$ tetrahedra to $^1_\infty[UO_5]^{4-}$ chains of edge-shared UO_7 pentagonal bipyramids alternately parallel to the $\vec{a}$- and $\vec{b}$-axis. By sharing an opposite corner the VO_4 tetrahedra can also create the divanadate V_2O_7 entity uncommon in the uranyl vanadate chemistry. Therefore two examples are known up today, $(UO_2)_2V_2O_7$ [26,27], and recently the layered compound $Cs_4(UO_2)_2(V_2O_7)O_2$ [28]. Thus, in this work we present the synthesis and the crystal structure of a new uranyl vanadate containing V_2O_7 divanadate groups, the lead uranyl divanadate $Pb(UO_2)(V_2O_7)$.

2. Experimental

2.1. Synthesis

The single crystal used for X-ray diffraction experiments was synthesized by solid-state reaction of PbO ((Johnson Matthey), V_2O_5 (Aldrich) and U_3O_8 (Prolabo), which were placed in a platinum crucible in the metallic ratio Pb:V:U = 1:6:2. After the grinding of the reagents in agate mortar, the crucible and its content were heated in air to 680 °C where the temperature was maintained for 2 h and then slowly cooled to room temperature at 5 °C h^{-1}. After washing of the obtained yellowish shiny crystalline product with ethanol, yellow crystals of $Pb(UO_2)V_2O_7$ phase were obtained.

The powder of this compound was also prepared by conventional solid-state reactions, using pure initial materials PbO, V_2O_5 and U_3O_8 according the following reaction:

$$PbO + V_2O_5 + 1/3U_3O_8 + 1/6O_2 \rightarrow Pb(UO_2)(V_2O_7)$$

Mixed starting materials in the appropriate stochiometries were heated at 570 °C in air for three days with intermediate grindings. The end of the synthesis process was controlled by X-ray powder diffraction using a Guinier–De Wolff focusing camera and Cu$K\alpha$ radiation. The X-ray diffraction pattern of the as-obtained powder is identical to that of crushed single crystals and to that of the calculated pattern from the crystal structure results.

The parameters of the monoclinic unit cell of $Pb(UO_2)(V_2O_7)$ were refined by a least-square procedure from powder X-ray diffraction data recorded at room temperature on a Siemens D5000 diffractometer using a Bragg–Brentano geometry with a back end monochromatized Cu$K\alpha$ radiation and corrected for $K\alpha_2$ contribution. The refined powder X-ray diffraction pattern data with the figure of merit F_{20} as defined by Smith and Snyder [29] and the refined unit cell parameters, are reported in Table 1.

Using the polycrystalline sample, the density measured with an automated Micromeritics Accupyc 1330 helium pycnometer shows the very good agreement between calculated and measured density, obtained with $Z = 4$ formula per unit cell ($\rho_{mes} = 5.82(3)$ and $\rho_{cal} = 5.83(1)\,g\,cm^{-3}$).

2.2. Thermal analysis

To study the thermal stability of the compound, a differential thermal analysis (DTA) was performed in air with a SETARAM 92–1600 thermal analyzer in the temperature range of 20–1000 °C with heating and cooling rate of 1.5 °C/min, using platinum crucibles. Thus, an endothermic peak observed at about 710 °C indicates a congruent melting point of $Pb(UO_2)(V_2O_7)$ compound. The powder X-ray diffraction analysis of residue after DTA measurement, confirms the only existence of a single phase of $Pb(UO_2)(V_2O_7)$.

2.3. Single crystal X-ray diffraction

A well shape single crystal of $Pb(UO_2)(V_2O_7)$ with indexed faces indicated in Table 2, was mounted on a glass fiber and aligned on a Brucker SMART APEX CCD X-ray diffractometer. After preliminary determination of the cell parameters from 98 reflections, crystal X-ray diffraction intensities were collected by a combination of three sets of 600 frames using Mo$K\alpha$ ($\lambda = 0.71073$ Å) radiation selected by a graphite monochromator. The individual frames were measured using

Table 1
Observed and calculated X-ray powder diffraction pattern for $PbUO_2V_2O_7$

hkl	$2\theta_{obs}$	$2\theta_{calc}$	I_{obs}/I_o	*hkl*	$2\theta_{obs}$	$2\theta_{calc}$	I_{obs}/I_o
1 0 −1	14.651	14.647	2	2 2 −3	38.912	38.909	1
1 0 1	15.036	15.042	2	3 0 −1	39.570	39.568	5
1 1 0	15.754	15.756	23	1 0 −5	40.015	40.022	1
1 1 −1	17.304	17.300	4	3 1 0	40.188	40.179	9
0 1 2	17.631	17.632	23	0 4 2	40.360	40.366	7
1 1 1		17.638		1 4 1		40.368	
0 2 0	18.373	18.376	4	2 1 −4	40.695	40.688	5
0 2 1	19.877	19.872	3	2 0 4	40.812	40.810	2
1 1 −2	21.562	21.568	20	3 1 1	41.159	41.164	2
1 1 2	22.121	22.112	18	0 3 4	41.541	41.540	2
1 2 0	22.468	22.452	7	2 3 2		41.550	
0 2 2	23.818	23.823	100	1 1 5	41.895	41.907	2
0 1 3	24.454	24.459	21	2 1 4	41.895	41.914	2
1 0 −3	25.734	25.730	5	1 4 −2	42.368	42.363	2
1 0 3	26.435	26.421	3	1 4 2	42.667	42.662	6
1 2 −2	26.897	26.905	3	0 2 5		42.674	
2 1 0	27.370	27.374	8	3 1 −2		42.682	
1 1 3	28.006	28.017	4	1 3 −4	43.351	43.346	10
2 1 −1	28.188	28.208	2	3 1 2	43.565	43.570	3
2 1 1	28.637	28.633	10	0 4 3	44.012	44.014	1
0 3 1	28.739	28.747	8	3 2 1	44.408	44.388	5
0 2 3	29.307	29.304	5	2 3 −3		44.402	
2 0 −2	29.525	29.531	15	1 2 5	45.100	45.088	10
0 0 4	30.341	30.329	21	2 2 4		45.095	
2 0 2		30.342		2 3 3	45.279	45.263	12
1 3 0	30.624	30.627	10	2 4 0	45.836	45.818	2
2 1 −2	30.987	30.980	9	3 2 −2		45.820	
1 3 −1	31.475	31.479	1	3 0 3	46.231	46.221	3
1 3 1	31.665	31.672	2	2 4 −1	46.360	46.358	2
0 1 4	31.735	31.745	7	2 4 1	46.619	46.637	1
2 2 0	31.796	31.810	20	3 2 2	46.664	46.661	2
1 2 3	32.375	32.372	2	3 1 3	47.210	47.224	3
2 2 −1	32.545	32.540	1	0 3 5	47.799	47.814	5
2 2 1	32.905	32.914	2	2 4 −2	48.227	48.220	5
1 1 −4	34.005	33.990	1	2 1 5	48.290	48.285	5
1 3 2	34.466	34.459	6	1 1 −6	48.704	48.709	6
1 1 4	34.712	34.707	5	0 4 4	48.763	48.752	8
2 2 −2	35.012	35.002	3	2 4 2		48.761	
0 4 0	37.259	37.238	3	3 2 −3	48.927	48.943	2
0 4 1	38.056	38.040	2	1 5 0		48.953	
1 2 4	38.389	38.385	2	2 3 −4	48.970	48.977	4
1 3 3	38.646	38.657	1	1 5 −1	49.527	49.532	1
2 3 −1	38.805	38.801	2	2 2 −5	49.844	49.844	1

Note. $\lambda = 1.54056$ Å, refined zero-point correction 0.01(1) for 2θ; $a = 6.9216(8)$ Å, $b = 9.653(1)$ Å, $c = 11.787(1)$ Å, $\beta = 91.737(2)^\circ$; $F_{20} = 137(0.0054; 27)$.

a ω-scan technique with an omega rotation of 0.3° and an acquisition time of 40 s per frame. Thus, a total of 1800 frames were collected. After data collection, the diffracted reflections intensities were reduced and corrected for Lorentz, polarization and background effects with the Brucker SAINTPLUS (v. 6.02) software package [30] using a narrow-frame integration algorithm. Once the data processing was performed, a face-indexed analytical absorption correction was applied by the Gaussian method using XPREP program [31], followed by a semi-empirical absorption correction by SADABS [32], in point group $2/m$. The unit cell parameters refined from all collected reflections with the summaries of the crystal data, details concerning the intensity data collection and structure refinements are given in Table 2. Examination of the systematic absences ($0k0$: $k = 2n + 1$ and $h0l$: $h + l = 2n + 1$) led to the choice of $P2_1/n$ space group, which is an unconventional setting of $P2_1/c$. The crystal structure was solved by direct methods using the XS program of SHELXTL software package [31], which localizes the heavy atoms U and Pb. Vanadium and oxygen atom positions were deduced from subsequent refinements and difference Fourier maps calculation. Then the

Table 2
Crystal data, intensity collection and structure refinement parameters for $PbUO_2V_2O_7$

Crystal data	Monoclinic			
Crystal symmetry	$P2_1/n$			
Space group	$a=6.9212(9)$Å			
Unit cell parameters	$b=9.6523(13)$Å			
	$c=11.7881(16)$Å			
	$\beta=91.74(1)^\circ$			
	$V=787.2(2)$Å^3			
Z	4			
Calculated density	$\rho_{cal}=5.83(1)$g/cm^3			
Measured density	$\rho_{mes}=5.82(3)$g/cm^3			
Data collection				
Temperature (K)	293(2)			
Equipment	Bruker SMART CCD			
Radiation Mo$K\alpha$	0.71073Å			
Scan mode	ω			
Recording angular range(deg)	2.73–31.50			
Recording reciprocal space	$-9\leqslant h\leqslant 10$			
	$-13\leqslant k\leqslant 14$			
	$-16\leqslant l\leqslant 17$			
No. of measured reflections	7462			
No. of independent reflections	2136			
R merging factor	0.042			
μ (cm^{-1}) (for $\lambda_{K\alpha}=0.71073$Å)	441.56			
Limiting faces and distances (mm)	0−10	0.025	−100	0.055
From an arbitrary origin	011	0.052	1−10	0.008
	521	0.062	01−2	0.010
	001	0.044		
Refinement				
Refined parameters/restraints	119/0			
Goodness of fit on F^2	1.106			
$R_1[I>2\sigma(I)]$	0.029			
w$R_2[I>2\sigma(I)]$	0.063			
R_1 for all data	0.033			
wR_2 for all data	0.065			
Largest diff. peak/hole(eÅ^{-3})	3.02/-1.81			

Note. $R_1=\Sigma(|F_o|-|F_c|)/\Sigma|F_o|$, $wR_2=[\Sigma w(F_o^2-F_c^2)^2/\Sigma w(F_o^2)^2]^{1/2}$, $w=1/[\sigma^2(F_0^2)+(aP)^2+bP]$ where a and b are refinable parameters and $P=(F_o^2+2F_c^2)/3$.

crystal structure was refined on the basis of F^2 for all unique data, using the XL program [31]. In the last cycles of refinement, anisotropic thermal displacements for all atoms were considered and an optimized weighting scheme yielded the final $R_1=0.029$ and $wR_2=0.064$. Tables 3 and 4 list the atomic positions with equivalent isotropic displacement parameters and anisotropic thermal displacement parameters, respectively.

2.4. Lone-pair electrons localization

The lead cation Pb^{2+} possessing an external electronic configuration ns^2np^0, it results the presence of lone-pair electrons and the polarization of the lead cation. The lone-pair electrons localization was carried out using the program Hybride [33] based on the algorithm of Verbaere et al. [34], in which the local crystal field (E) is calculated by the Ewald's method [35], where the

Table 3
Atomic positions and isotropic equivalent displacement parameters for $Pb(UO_2)V_2O_7$

Atom	Site	x	y	z	U_{eq}(Å^2)[a]
U	4*e*	0.96024(4)	0.49579(3)	0.22698(2)	0.01025(9)
Pb	4*e*	0.20084(5)	0.19000(3)	0.03563(3)	0.0171(1)
V(1)	4*e*	0.7202(2)	0.22611(9)	0.03511(9)	0.0110(3)
V(2)	4*e*	0.4100(2)	0.53992(9)	0.16904(9)	0.0105(3)
O(1)	4*e*	0.6309(9)	0.4941(6)	0.2216(5)	0.018(1)
O(2)	4*e*	0.2588(8)	0.4052(6)	0.1393(5)	0.016(1)
O(3)	4*e*	0.2757(8)	0.6156(6)	0.2693(5)	0.016(1)
O(4)	4*e*	0.8310(9)	0.1032(7)	0.9647(5)	0.022(1)
O(5)	4*e*	0.9059(8)	0.3044(6)	0.1093(5)	0.015(1)
O(6)	4*e*	0.5835(9)	0.3531(6)	0.9536(5)	0.018(1)
O(7)	4*e*	0.9635(9)	0.3751(6)	0.3383(5)	0.020(1)
O(8)	4*e*	0.9428(9)	0.6200(7)	0.1151(5)	0.021(1)
O(9)	4*e*	0.5616(9)	0.1539(6)	0.1265(6)	0.022(1)
Lp[b]	4*e*	0.228(9)	0.184(8)	−0.008(7)	

[a]The U_{eq} values are defined by $U_{eq}=1/3(\sum_i\sum_j U_{ij}a^*_i a^*_j a_i a_j)$.
[b]Lp: Lonepair.

Table 4
Anisotropic displacement parameters (Å^2) for $Pb(UO_2)V_2O_7$

Atom	U_{11}	U_{22}	U_{33}	U_{12}	U_{13}	U_{23}
U	0.00893(9)	0.01108(9)	0.01071(9)	0.00049(9)	−0.00045(9)	0.00001(9)
Pb	0.01733(9)	0.01881(9)	0.01525(9)	0.00270(9)	0.00117(9)	0.00080(9)
V(1)	0.0091(6)	0.0109(6)	0.0130(7)	−0.0013(5)	−0.0002(5)	0.0009(5)
V(2)	0.0079(6)	0.0117(6)	0.0120(6)	0.0003(5)	−0.0006(5)	0.0003(5)
O(1)	0.012(3)	0.021(3)	0.020(3)	−0.001(2)	−0.005(2)	0.001(3)
O(2)	0.014(3)	0.010(3)	0.023(3)	−0.002(2)	−0.001(2)	0.000(2)
O(3)	0.016(3)	0.021(3)	0.012(3)	0.002(2)	0.001(2)	−0.004(2)
O(4)	0.027(3)	0.019(3)	0.019(3)	0.003(3)	−0.002(3)	−0.008(3)
O(5)	0.011(3)	0.021(3)	0.015(3)	−0.004(2)	−0.001(2)	−0.005(2)
O(6)	0.019(3)	0.016(3)	0.018(3)	−0.001(2)	−0.002(2)	0.000(2)
O(7)	0.024(3)	0.019(3)	0.018(3)	0.003(3)	0.004(3)	0.003(3)
O(8)	0.020(3)	0.020(3)	0.021(3)	−0.002(3)	0.001(3)	0.006(3)
O(9)	0.018(3)	0.023(3)	0.025(4)	−0.001(3)	0.005(3)	0.014(3)

Note. The anisotropic temperature factor is defined by $\exp[-2\pi^2(U_{11}h^2a^{*2}+\cdots+2U_{23}klb^*c^*)]$.

electronic polarizability for Pb^{2+} was chosen as $\alpha = 6.583$ Å^3 [36]. The calculation used to determine ions partial charges derives from the Pauling empirical formula [37], that gives the ionicity rate of a Metal–Oxygen bond M–O according to the difference between the electronegativity χ_M and χ_O of metal and oxygen atoms. Values of χ are taken in the electronegativity scale of Allred et al. [34]. Thus, a % formal ionicity value (FI_{M-O}) was calculated for each bond using the formula:

$$FI_{M-O} = 1 - \exp\frac{\chi_O - \chi_M}{4},$$

Thus, the formal charge Q' used for each atom is obtained by the following expression: $Q' = FI_{M-O} \times Q$, where Q is −2, +2, +5 and +6 for oxygen, lead, vanadium and uranium atoms, respectively. Thus, the refined coordinates of the lone-pair position are given in Table 3.

2.5. Infrared spectroscopy

The infrared spectrum was recorded using the KBr dispersion technique (1 mg of sample in 125 mg KBr) with a Bruker Vector 22 Fourier Transform Infrared Spectrometer, which covers the range 400–4000 cm^{-1}.

3. Description of the structure and discussion

Select bond distances with uranyl ion angle and bond valence sums calculated using Brese and O'Keeffe data [38], except for U–O bonds where the coordination independent parameters were taken from Burns et al. [39], are given in Table 5.

$Pb(UO_2)(V_2O_7)$ is a three-dimensional framework material composed by edge- and corner-sharing of U- and V-centered polyhedra creating elliptic tunnels running down the [110] direction and occupied by Pb^{2+} ions (Fig. 1).

The unique independent uranium atom is bonded to two oxygen atoms at short distances, 1.754(6) and 1.784(6) Å for O(7) and O(8), respectively, forming a nearly linear uranyl ion UO_2^{2+} (O–U–O = 176.8(3)°) which is surrounded in the equatorial plane by a pentagonal environment of five crystallographically independent oxygen atoms at distances in the range 2.278(6)–2.507(6) Å, Fig. 2a. Thus, the uranium atom coordination is a pentagonal bipyramid $(UO_2)O_5$ which represent the most frequent case for U^{6+} environment. There are two independent vanadium atoms V(1) and V(2), having a strongly distorted tetrahedral coordination. The V(1) environment is defined by O(4) atom at shorter distance (1.650(7) Å), O(5) and O(9) at intermediate and nearly equal distances 1.709(6) and 1.710(7) Å, respectively, and finally O(6) at 1.807(6) Å. For V(2), O(1) and O(3) are at the same short distance, 1.691(6) Å, O(2) at 1.699(6) Å and finally O(6) at 1.778(6) Å. $V(1)O_4$ and $V(2)O_4$ tetrahedra share the O(6) corners to form a V_2O_7 divanadate unit with a non-linear angle V(1)–O(6)–V(2) of 143.2(4)°, the V–O(6) distances are the longer for both V(1) and V(2), Fig. 2b. The bridging V–O–V angle in V_2O_7 divanadate units vary from perfectly linear as, for example, in $U_2V_2O_{11}$ (26,27) to 122° in $Pb_2V_2O_7$ [40]. The Pb atom is surrounded by eight oxygen ions at distances less than or equal to 3.06 Å (Fig. 2c), three on one side at short distances and the others on the other side at longer distances. The Lp lone pair is pointing toward the empty space opposite to the three shortest Pb–O bonds, with Pb^{2+}–Lp distance of 0.561 Å, Fig. 2c. As commonly

Table 5
Selected bond distances (Å), angles (deg) and bond valences for $Pb(UO_2)V_2O_7$

U environment				*Pb environment*		
Uranyl ion angle					d_{Pb-O}	s_{ij}
O(7)–U–O(8)	176.8(3)			Pb–(O3)^{iii}	2.410(6)	0.447
	d_{U-O} (Å)	s_{ij}		Pb–(O2)	2.437(6)	0.415
U–O(7)	1.754(6)	1.772		Pb–(O5)^{iv}	2.500(6)	0.351
U–O(8)	1.784(6)	1.673		Pb–(O9)	2.709(7)	0.199
U–O(1)	2.278(6)	0.644		Pb–(O8)^{v}	2.721(6)	0.193
U–O(9)^{i}	2.313(7)	0.604		Pb–(O4)^{ix}	2.797(6)	0.157
U–O(5)	2.334(6)	0.580		Pb–(O4)^{x}	2.839(7)	0.140
U–O(2)^{ii}	2.497(6)	0.423		Pb–(O7)^{viii}	3.061(7)	0.077
U–O(3)^{ii}	2.507(6)	0.415				
$\sum s_{ij}$		6.111				1.980
V environment						
Divanadate angle						
V(1)–O(6)–V(2)	143.2(4)					
	d_{V-O}(Å)	s_{ij}			d_{V-O}	s_{ij}
V(1)–O(4)^{vi}	1.650(7)	1.512		V(2)–O(1)	1.691(6)	1.354
V(1)–O(5)	1.709(6)	1.289		V(2)–O(3)	1.691(6)	1.354
V(1)–O(9)	1.710(7)	1.286		V(2)–O(2)	1.699(6)	1.325
V(1)–O(6)^{vi}	1.807(6)	0.987		V(2)–O(6)^{vii}	1.778(6)	1.070
$\sum s_{ij}$		5.074				5.103
Lp environment						
	d_{Lp-O}(Å)		d_{Lp-O}(Å)			
Lp–Pb	0.561(14)	Lp–O(4)^{x}	2.854(16)			
Lp–O(7)^{viii}	2.534(14)	Lp–O(4)^{ix}	2.866(12)			
Lp–O(8)^{v}	2.541(15)	Lp–O(3)^{iii}	2.898(15)			
Lp–O(2)	2.758(15)	Lp–O(5)^{iv}	2.904(14)			
Lp–O(9)	2.779(13)	Lp–O(6)^{vi}	2.995(13)			

Note. Symmetry codes: (i) $1.5-x$, $0.5+y$, $0.5-z$; (ii) $1+x$, y, z; (iii) $0.5-x$, $-0.5+y$, $0.5-z$; (iv) $-1+x$, y, z; (v) $1-x$, $1-y$,$-z$; (vi) x, y, $-1+z$; (vii) $1-x$,$1-y$, $1-z$; (viii) $-0.5+x$, $0.5-y$, $-0.5+z$; (ix) $-1+x$, y, $-1+z$; (x) $1-x$, $-y$, $1-z$.

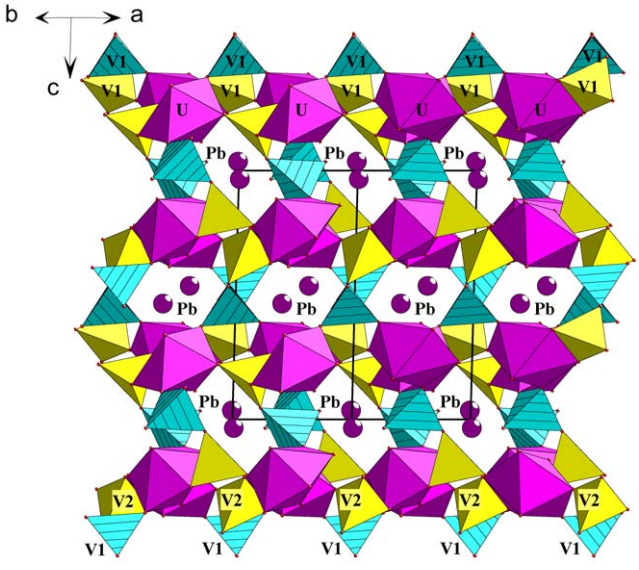

Fig. 1. Projection of the crystal structure of $PbUO_2(V_2O_7)$ along the [110] direction showing the three-dimensional framework of corner and edge shared UO_7 pentagonal bipyramids and VO_4 tetrahedra creating elliptic one-dimensional channels occupied by Pb^{2+} ions.

observed, this distance is shorter than the Pb^{2+} ionic radius. One should consider the $6s^2$ pair as an excrescence of peripheral electronic levels partially *sp* hybridized. On the basis of the U–O, V–O and Pb–O bond lengths, bond valence sums were calculated to be 6.11, 5.07, 5.10, 1.98, for U, V(1), V(2) and Pb, respectively. These values are in agreement with the expected values. Bond valence sums for the O atoms range from 1.82 to 2.22.

Although the overall structure has three-dimensional connectivity, it may be instructional in the first instance to consider it as having layers of UO_7 pentagonal bipyramids and VO_4 tetrahedra in the (001) plane, which are further linked into three dimensions along *c* via the formation of divanadate entities. The UO_7 pentagonal bipyramids do not share directly any anion but are connected through sharing O(5) and O(9) corners with $V(1)O_4$ tetrahedra to form infinite $^{1}_{\infty}[UV(1)O_9]$ zig-zag chains running down the $\vec{b}$-axis, Fig. 3. In addition each UO_7 polyhedron is linked to two other $V(2)O_4$ tetrahedra, one by sharing corners and one by sharing edges. Thus two consecutive zig-zag chains are connected together through $V(2)O_4$ tetrahedra to form corrugated $^{2}_{\infty}[UV_2O_9]^{-}$ layers parallel to (001) with a new anion-topology [41]. The condensation of $V(1)O_4$ and $V(2)O_4$ tetrahedra between two parallel layers by sharing the O(6) corners leads to the three-dimensional framework.

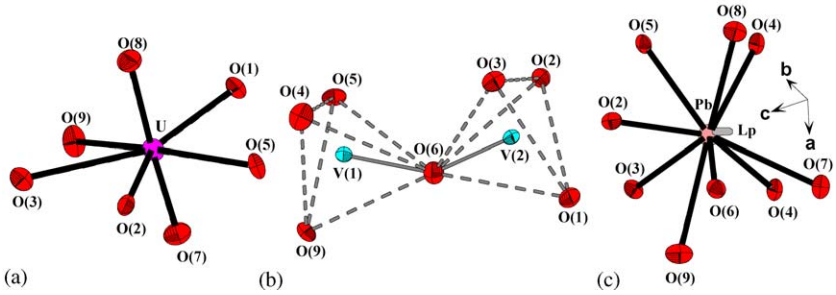

Fig. 2. The oxygen polyhedra around (a) the uranium atom, (b) the vanadium atoms showing the divanadate entity formed by vanadium tetrahedra sharing corner, (c) the Pb^{2+} ion showing the Lp calculated lone-pair electron position.

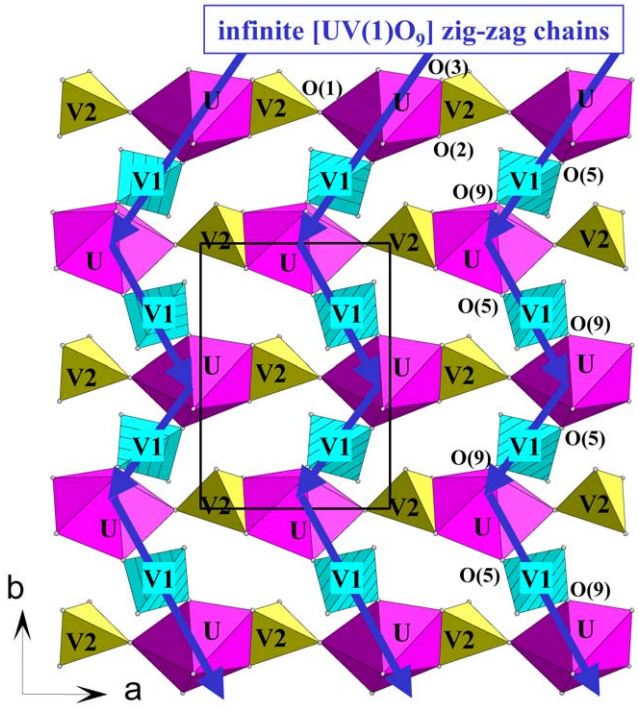

Fig. 3. View on the (001) plane of the infinite parallel $^1_\infty[UV(1)O_9]$ zig-zag chains running down the $\vec{b}$-axis and connected through the $V(2)O_4$ tetrahedra to form corrugated $^2_\infty[UV_2O_9]^-$ layers.

If only the seven Pb–O distances lower than 3 Å are considered, the Pb environment can be described as a deformed pentagon with O(2), O(5), O(9), and two O(4) oxygen atoms, completed by O(3) and O(8) atoms to form a very distorted pentagonal bipyramidal environment which becomes comparable to that of uranyl ion. It is thus possible to consider two types of similar chains parallel to $\vec{a}$-axis, $^1_\infty[PbV(1)O_8]$ and $^1_\infty[UV(2)O_8]$ chains, Fig. 4a. The association of these chains by equatorial edges sharing between UO_7 and PbO_7 pentagonal bipyramids in the sequence $[UV(2)O_8]$–$[PbV(1)O_8]$–$[PbV(1)O_8]$–$[UV(2)O_8]$ gives an infinite four polyhedra wide ribbon, $^1_\infty[Pb_2(UO_2)_2(VO_4)_4O_6]$ which can be also described by $Pb_2U_2V_4O_{30}$ tetramers connected to each other by sharing corners, Fig. 4a. The infinite ribbons are connected together to form the three-dimensional framework. It is interesting to compare the ribbons found in $Pb(UO_2)V_2O_7$ with the sheets based on the uranophane-anion topology [41] found in many uranyl-containing compounds and in particular in the uranyl divanadate $(UO_2)_2V_2O_7$ Fig. 4b. In $Pb(UO_2)V_2O_7$ half the U atoms are replaced by Pb, Fig. 4b.

The infrared spectrum (400–1100 cm^{-1}) of $Pb(UO_2)(V_2O_7)$, Fig. 5, is characterized by vibrations of uranyl UO_2 and divanadate V_2O_7 groups. For the interpretation of this spectrum the following building units have been considered: UO_2^{2+} groups, equatorial (secondary) U–O bonds in pentagonal environment, V_2O bridges and terminal VO_3 groups. The spectrum shows two strong bands at about 888 and 810 cm^{-1}, which can be attributed to asymmetrical and symmetrical UO_2^{2+} uranyl stretching vibrations ν_3 and ν_1, respectively. These two vibrations are in good agreement with the mathematical model suggested by Bagnall et al. [42] to determine the value of ν_1 from the one of ν_3, given by the following expression:

$$\nu_1 = 0.912\nu_3 - 1.04\,cm^{-1}.$$

Thus, the application of Veal et al.'s empirical equation [43], relating bond length (R) to the asymmetric stretching vibration ν_3 (888 cm^{-1}) for uranyl groups:

$$R_{U-O} = 81.2\nu 3^{-2/3} + 0.895$$

leads to the predicted uranyl bond length of 1.77 Å, in good agreement with the average value obtained from X-ray structure results, $\langle$U–O$\rangle$1.769(6)Å. The lower bands observed in the range 440–600 cm^{-1} may be assigned to the $U–O_{eq}$ vibrations between uranium and equatorial oxygen atoms, these bands were also observed in other mineral and inorganic compounds

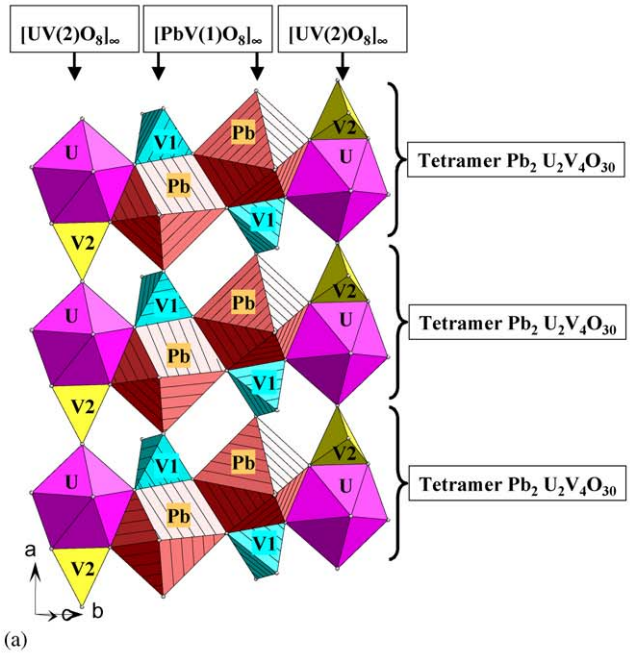

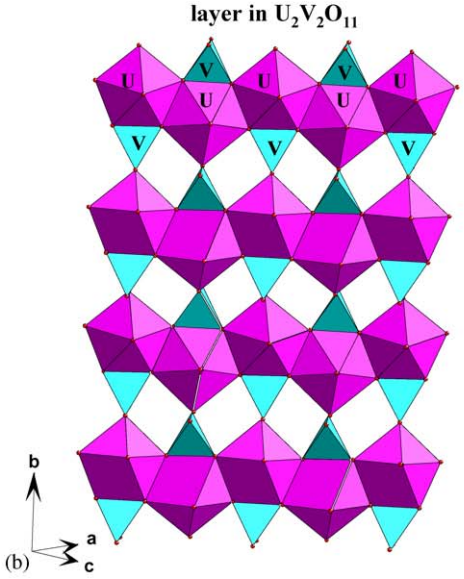

Fig. 4. View of (a) the $^{1}_{\infty}[Pb_2(UO_2)_2(VO_4)_4O_6]$ infinite four bipyramids wide ribbon of $PbUO_2(V_2O_7)$ showing the $Pb_2U_2O_{30}$ tetramers of edge shared UO_7 and PbO_7 pentagonal bipyramids connected together by VO_4 tetrahedra compared to (b) the sheet of uranophane type anion-topology in $(UO_2)(V_2O_7)$ formed by infinite UO_5 chains of edge shared UO_7 and PbO_7 pentagonal bipyramids connected together by VO_4 tetrahedra.

[44]. In addition, the two bands at 920 and 980 cm^{-1} correspond to VO_3 symmetric stretch, whereas, those observed in the range 727–770 and at 840 and 875 cm^{-1} to VO_3 asymmetric stretch and finally the weak shoulder observed at about 635 cm^{-1} can be attributed to V–O–V

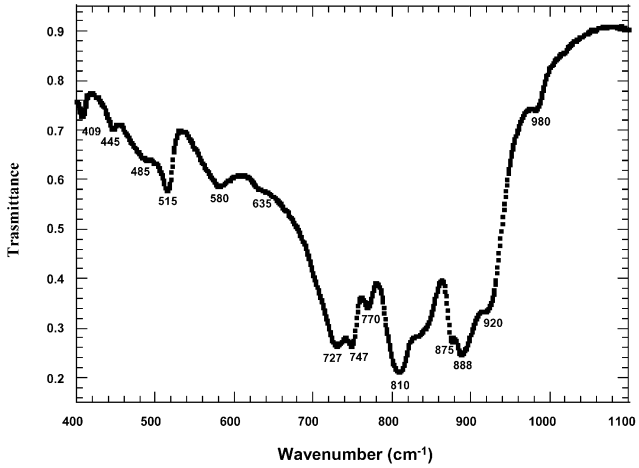

Fig. 5. Infrared spectrum of $PbUO_2(V_2O_7)$.

Table 6
Infrared absorption bands in $Pb(UO_2)V_2O_7$

Wave number (cm^{-1})	Vibrational mode
810	$\nu_1(UO_2^{2+})$ symmetric stretching
888	$\nu_3(UO_2^{2+})$ asymmetric stretching
410–445–485–515–580	$\nu(U–O_{eq})$ equatorial vibrations
920–980	$\nu_1(VO_3)$ symmetric stretching
727–747–770	$\nu_3(VO_3)$ asymmetric stretching
635	(V–O–V) bridges vibrations

bridges [44]. A summary of the assignment of the absorption bands is given in Table 6.

References

[1] G. Branche, M.E. Ropert, F. Chautret, F. Moricnat, R. Pouget, C.R. Acad, Sci. Fr. 245 (1957) 89.
[2] V.P. Rogova, G.A. Sidorenko, N.N. Kusnetsova, Zap. Vser. Mineral. Obshchest. SSSR 95 (4) (1966) 448.
[3] F. Cesbron, N. Morin, Bull. Soc. Fr. Minéral. Cristallogr. 91 (5) (1968) 453.
[4] F. Cesbron, J. Borène, Bull. Soc. Fr. Minéral. Cristallogr. 94 (1) (1971) 8.
[5] D.P. Shashkin, Dokl. Akad. Nauk. SSSR 220 (6) (1975) 1410.
[6] K. Mereiter, Neues Jahrbuch Mineral. Monatshefte 12 (1986) 552.
[7] M. Saadi, Thèse de Doctorat, Lille, 1994.
[8] F. Abraham, C. Dion, M. Saadi, J. Mater. Chem. 3 (5) (1993) 459.
[9] M.A. Carnot, C.R. Acad. Sci. Paris 104 (1887) 1850.
[10] P.B. Barton, Am. Mineral. 43 (1958) 799.
[11] I.G. Smyslova, Zap. Vser. Mineral. Obshchest. SSSR 101 (1) (1972) 87.
[12] M.A. Alekseeva, A.A. Chernikov, D.P. Shashkin, E.A. Kon'kova, I.N. Gavrilova, Zap. Vser. Mineral. Obshchest. SSSR 103 (5) (1974) 576.
[13] K.J. Wenrich, P.J. Modreski, R.A. Zielinski, J.L. Seeley, Am. Mineral. 67 (11–12) (1982) 1273.
[14] D.E. Appleman, H.T. Evans, Am. Mineral. 50 (7–8) (1965) 825.
[15] G.P. Dickens, P. Garry, J. Mater. Chem. 2 (2) (1992) 161.
[16] F. Cesbron, Bull. Soc. Fr. Minéral. Cristallogr. 93 (3) (1970) 320.

[17] J.F. Vaes, P.F. Kerr, Am. Mineral. 34 (1949) 109.
[18] P. Piret, J.P. Declerco, D. Wauters-Stoop, Bull. Mineral. 103 (1980) 176.
[19] I. Duribreux, C. Dion, F. Abraham, M. Saadi, J. Solid State Chem. 146 (1999) 258.
[20] A.M. Chippindale, S.J. Crennell, P.G. Dickens, J. Mater. Chem. 3 (1993) 33.
[21] M. Saadi, C. Dion, F. Abraham, J. Solid State Chem. 150 (2000) 72.
[22] C. Dion, S. Obbade, E. Raekelboom, F. Abraham, M. Saadi, J. Solid State Chem. 155 (2000) 342.
[23] S. Obbade, C. Dion, L. Duvieubourg, M. Saadi, F. Abraham, J. Solid State Chem. 173 (2003) 1.
[24] I. Duribreux, M. Saadi, S. Obbade, C. Dion, F. Abraham, J. Solid State Chem. 172 (2003) 351.
[25] S. Obbade, C. Dion, M. Rivenet, M. Saadi, F. Abraham, J. Solid State Chem. 177 (2004) 2058.
[26] A.M. Chippindale, P.J. Dickens, G.J. Flynnand, G.P. Stuttard, J. Mater. Chem. 5 (1) (1995) 141.
[27] N. Tancret, S. Obbade, F. Abraham, Eur. J. Solid State Inorg. Chem. 32 (1995) 195.
[28] S. Obbade, C. Dion, M. Saadi, F. Abraham, J. Solid State Chem. 177 (2004) 1567.
[29] G. Smith, R.J. Snyder, J. Appl. Crystallogr. 12 (1979) 60.
[30] SAINT Plus version 5.00, Bruker Analytical X-ray Systems, Madison, WI, 1998.
[31] G.M. Sheldrick, SHELXTL PC, Version 6.12, An Integrated System for Solving, Refining, and Displaying Crystal Structures from Diffraction Data, Siemens Analytical X-ray Instruments, Inc., Madison, WI, 2001.
[32] R.H. Blessing, SADABS, Program for absorption correction using SMART CCD based on the method of Blessing, 1995.
[33] E. Morin, G. Wallez, S. Jaulmes, J.C. Couturier, M. Quarton, J. Solid State Chem. 137 (1998) 283.
[34] A. Verbaere, R. Marchandm, M.J. Tournoux, J. Solid State Chem. 23 (1978) 383.
[35] P.P. Ewald, Ann. Phys. 64 (1921) 253.
[36] R.D. Shannon, J. Appl. Phys. 73 (1) (1993) 348.
[37] L. Pauling, The Nature of the Chemical Bond, Cornell University Press, New York, 1939.
[38] N.E. Brese, M. O'Keeffe, Acta Crystallogr. B 47 (1991) 192.
[39] P.C. Burns, R.C. Ewing, F.C. Hawthorne, Can. Mineral. 35 (1997) 1551.
[40] R.D. Shannon, C. Calvo, Can. J. Chem. 51 (1973) 70.
[41] P.C. Burns, M.L. Miller, R.C. Ewing, Can. Mineral. 34 (1996) 845.
[42] K.W. Bagnall, M.W. Wakerley, J. Inorg. Nucl. Chem. 37 (1) (1975) 329.
[43] B.W. Veal, D.J. Lam, W.T. Carnall, H.R. Hestra, Phys. Rev. B (1975) 5651.
[44] J. Cejka, Rev. Miner. 38 (1999) 221.